

Resonance Energy Transfer between Green Fluorescent Protein Variants: Complexities Revealed with Myosin Fusion Proteins[†]

Wei Zeng,^{‡,§} Harriet E. Seward,[‡] András Málnási-Csizmadia,^{‡,||} Stuart Wakelin,[‡] Robert J. Woolley,^{‡,⊥} Gurpreet S. Cheema,[‡] Jaswir Basran,[‡] Trushar R. Patel,[#] Arthur J. Rowe,[#] and Clive R. Bagshaw^{*,‡}

Department of Biochemistry, University of Leicester, Leicester LE1 9HN, U.K., and National Centre for Macromolecular Hydrodynamics, University of Nottingham, Sutton Bonington, Leicestershire LE12 5RD, U.K.

Received May 12, 2006; Revised Manuscript Received July 13, 2006

ABSTRACT: Green fluorescent protein and its variants are frequently used as Förster (fluorescence) resonance energy transfer (FRET) pairs to determine the proximity of protein domains. We prepared fusion proteins comprising yellow fluorescent protein–*Dictyostelium* myosin II motor domain–cyan fluorescent protein (YFP–myosin–CFP) and compared their FRET properties with an existing construct (GFP–myosin–BFP), containing a green fluorescent protein acceptor and blue fluorescent protein donor [Suzuki, Y., Yasunaga, T., Ohkura, R., Wakabayashi, T. and Sutoh, K. (1998) *Nature* 396, 380–383]. The latter construct showed an apparent 40% reduction in acceptor fluorescence on ATP addition, when excited via the donor, compared with the YFP–myosin–CFP constructs which showed a small increase ($\leq 5\%$). We propose that this disparity primarily arises from the differential response of GFP and YFP on intramolecular association with the donor probe. Studies with isolated GFP and YFP at high concentrations show that they dimerize with similar K_d values but the spectrum shifts toward the protonated state only with GFP. On excitation at 380 nm, the protonated GFPH emits at 510 nm via excited-state proton transfer, giving the appearance of extensive FRET. These findings have important implications for FRET measurements using GFP-type probes because they give rise to changes in donor and acceptor emission ratios through processes other than FRET and complicate the extraction of the true degree of energy transfer from experimental data. Furthermore, the unknown orientation factor prevents the distance of the lever arm swing from being derived from these FRET changes.

Förster (fluorescence) resonance energy transfer between proteins derived from GFP¹ has become a widely used tool in cell biology to study protein interactions within living cells (1–5). These proteins have also been used as probes in vitro to investigate structural changes in macromolecular complexes. In many cases the FRET signal is used in an empirical way to determine if protein domains are within close proximity or not. However, in other instances the Förster equation is used in an attempt to quantify distances between

the probes (6–9). The use of GFP and its variants in the latter context presents some advantages and some problems (10). The principle advantages are that the sites to be probed can be labeled specifically and stoichiometrically, provided that the GFP folding and chromophore maturation are complete. The principle disadvantages are that the probes are bulky and the fluorophores are held rigidly within a β -barrel structure such that they cannot rotate significantly during the lifetime of fluorescence. Consequently, the orientation factor, κ^2 , is difficult to define, and there is no justification for assuming the value of $2/3$ that was derived for fluorophores freely and rapidly rotating over all orientations.

Another problematic area is the environmental sensitivity of GFP (11). It is well-known that the fluorophore of many GFP variants has a pK value close to physiological pH (2, 10). It is important to take this into account because the protonated and deprotonated forms have different absorption and fluorescence spectra. Some species are also sensitive to other ions [e.g., YFP is sensitive to Cl[−] (12)]. These factors are of particular concern in the development of intracellular FRET probes, such as those designed to measure Ca²⁺ concentrations. However, with in vitro studies where pH and ionic strength can be controlled, environmental factors are perceived to be less of a problem. Indeed, the protection of the fluorophore within the β -barrel structure of GFP appears to render it relatively immune from many environmental

[†] This work was supported by the Biotechnology and Biological Sciences Research Council and The Leverhulme Trust, U.K. A.M.-C. was supported by EMBO/HHMI and Békéssy fellowships, Wellcome Trust IRDA Scheme, KMÚFA-BIO-110/2002, OTKA TS047154, and National Office for Research and Technology RET 14/2005.

* To whom correspondence should be addressed. Tel: +44 (0)116 229 7048. Fax: +44 (0)116 229 7018. E-mail: crb5@le.ac.uk.

[‡] University of Leicester.

[§] Present address: Division of Medical Studies, The Medical School, University of Birmingham, Birmingham, U.K.

^{||} Present address: Department of Biochemistry, Eötvös Loránd University, H-1117 Budapest, Hungary.

[⊥] Present address: Department of Biomedical Sciences, University of Sheffield, Sheffield S10 2TN, U.K.

[#] University of Nottingham.

¹ Abbreviations: BFP, blue fluorescent protein; CFP, cyan fluorescent protein; ESPT, excited-state proton transfer; FRET, Förster (fluorescence) resonance energy transfer; *Dd*, *Dictyostelium discoideum*; GFP, green fluorescent protein; HEPES, *N*-(2-hydroxyethyl)piperazine-*N'*-2-ethanesulfonic acid; MES, 2-(*N*-morpholino)ethanesulfonic acid; MOPS, 3-(*N*-morpholino)propanesulfonic acid; YFP, yellow fluorescent protein.

factors, other than pH. The wavelength maxima of the absorption and fluorescence of GFP variants are generally independent of the protein to which they are fused. This situation contrasts with many small molecule probes whose fluorescence undergoes significant spectral shifts on binding to a protein. Consequently, in the latter case, the quantum yield and overlap integral of the donor and acceptor need to be measured for each complex, before the Förster equation can be applied. In contrast, the observed constancy of the absorption and emission wavelengths has encouraged publication of standard spectra of GFP and its variants for the purpose of FRET analysis (13, 14). This practice, however, contains tacit assumptions about the absorption coefficients and effective pK values that we demonstrate here are not always met.

Our interest in this topic arose from the work of Suzuki et al. (6), who probed the lever arm movement of myosin by measuring FRET between GFP and BFP attached to the N- and C-termini of the *Dictyostelium discoideum* (*Dd*) myosin II motor domain. They reported that ATP binding induced a large change in FRET, based on GFP-sensitized emission, which reverted back to the initial state on P_i release. They presented a quantitative analysis of the FRET changes and incorporated their findings into a swinging lever arm model for the myosin cross-bridge. Subsequently, we made similar *Dd* myosin fusion proteins based on YFP and CFP (15) and found FRET changes that were much smaller and in the opposite direction to those reported by Suzuki et al. (6). We have now made a direct comparison between these constructs, which reveals a number of complexities in the apparent FRET signals. These factors are potentially common to other GFP constructs and need to be considered in any quantitative analysis of FRET.

MATERIALS AND METHODS

Constructs. *Dd* myosin II motor domain fusion proteins were prepared containing an N-terminal YFP (Clontech EYFP variant 10C, Biosciences, Oxford, U.K.) and a C-terminal CFP (Clontech ECFP), the latter having a C-terminal His₈ tag. The myosin motor domain was based on the W501+ construct (16), which retained a single tryptophan at position 501, and mutations W36F, W432F, and W584F. The pDXA-W501 vector coding this protein was the start point for subsequent cloning. The vector was digested with *Bam*HI plus *Kpn*I (*Bam*HI excises W501), and the YFP sequence inserted as a *Kpn*I–*Bam*HI fragment. The CFP sequence was inserted by *Bam*HI–*Nsi*I digestion and ligation. Finally, the W501+ sequence was reinserted following *Bam*HI digestion and ligation. The YFP and CFP inserts were also prepared with C- and N-terminal triple glycine linkers, respectively, to give three variant fusion proteins, as shown in Figure 1. The pBIG plasmid coding for GFP–myosin–BFP [\equiv GFP–S1–BFP of Sasaki et al. (17)] was kindly provided by Dmitry Kudryashov and Kazuo Sutoh. In this construct the myosin motor domain contained the full complement of tryptophan residues. The linker regions were confirmed by sequencing and compared in Figure 1.

Dd AX2 cells were electroporated and myosin constructs purified by Ni affinity chromatography as described previously (16). Isolated YFP was prepared as described previously (18), and GFP was made by an analogous procedure.

Construct	acceptor protein	<i>Dd</i> myosin motor domain	donor protein
YFP–myosin–CFP (0L)	.. DELYK ---DPIHDR...	EAREQRLGS ---MVSKG..	
YFP–myosin–CFP (1L)	.. DELYK ---DPIHDR...	EAREQRLGSGGGM VSKG..	
YFP–myosin–CFP (2L)	.. DELYKGGGMD PPIHDR...	EAREQRLGSGGGM VSKG..	
GFP–myosin–BFP	.. DELYK GPQKDPPIHDR...	EAREQRLASGGG –VSKG..	

FIGURE 1: Comparison of the linker sequences in the constructs used in this study. Residues in bold refer to the native sequence of the GFP probe variants and the myosin motor domain (which terminates at R761). Dots represent the intervening sequence, and dashes represent absent residues. The YFP–myosin–CFP constructs are distinguished by the number of triple glycine linkers (0L, 1L, 2L).

Spectroscopic Measurements. Absorption spectra were recorded with a Cary 50 spectrophotometer (Varian Ltd., Walton on Thames, U.K.). Fluorescence spectra were recorded with an Eclipse fluorometer (Varian Ltd.) or an SLM 8000/48000 fluorometer with polarization optics (SLM Aminco, Urbana, IL). For absorbance measurements at high concentration, samples were measured in 1 mm path length cells or approximately 0.1 mm cells constructed from microscope slides and coverslip spacers. The latter was mounted in a front-faced mode for fluorescence spectroscopy. Stopped-flow measurements were carried out using an SX18MV instrument (Applied Photophysics Ltd., Leatherhead, U.K.) equipped with Xe and Hg-Xe lamps. This instrument was modified to allow dual-channel fluorescence detection so that donor and acceptor emission could be monitored simultaneously. Temperature-jump experiments were performed using a TJ-64 instrument with Joule heating (Hi-Tech Scientific, Salisbury, U.K.). GFP and YFP emission was measured using OG515 and OG530 cutoff filters, respectively. BFP emission was monitored using a WG395 cutoff filter in combination with a 460IK25 band-pass filter. CFP emission was monitored using a GG450 cutoff filter in combination with a 505IK25 band-pass filter. Tryptophan emission was monitored by a combination of WG320 and UG11 filters (all filters from Comar Instruments, Cambridge, U.K.). Assays were carried out in 40 mM NaCl, 20 mM HEPES or MOPS, and 2 mM MgCl₂ at pH 7.5 and 20 °C, unless otherwise stated. Further details of these methods have been given previously (19). GFP photobleaching was achieved using 125 mW irradiation at 488 nm from an argon ion laser (Model 35LAP431; Melles-Griot, Huntingdon, U.K.) with a 120 μ L sample in a 105.250-QS microcuvette (Hellma, Southend-on-Sea, U.K.). Concentrations of GFP and YFP were calculated using absorption coefficients of 57 mM⁻¹ cm⁻¹ (488 nm) and 83 mM⁻¹ cm⁻¹ (514 nm), respectively (10).

Analytical Ultracentrifugation. Sedimentation equilibrium analysis was performed at 20 °C in a Beckman XL-I analytical ultracentrifuge, using Rayleigh interferometric optics; 12 mm optical path length centerpieces were used in the cell. After the laser settings were optimized and initial scans were taken at 3000 rpm, a final rotor speed of 15000 rpm was selected. Scans were taken immediately after reaching speed and then every 60 min until equilibrium was attained. Final scans were accepted for analysis when no significant detectable changes could be found between successive scans. Data were logged to disk using the Beckman software. The final data set used for analysis was obtained by subtraction of the initial scan at speed from the last scan recorded: this procedure ensures that any minor

deviations from linearity and/or slight optical inhomogeneities in the system cancel out.

Local software (the INVEQ suite) was employed (20, 21) for analysis. This allows for an assessment of the degree of self-interaction (if any) between the principal species present: INVEQ is particularly sensitive in defining weak interactions (to $K_d = 100$ mM under optimal conditions). The parameters floated for fitting were the K_a interaction constant, the BM (second virial coefficient), and the baseline offset (E). The fixed reduced molecular mass (σ) was determined via SEDNTERP (below). The INVEQ suite operates within the general curve-fitting program pro Fit (Quantum Soft, Zürich, Switzerland). In the present case, it could be assumed that the lowest (monomeric) mass species present was of mass = 29022 Da. The reduced mass of this species (the σ value), the quantity actually determined in sedimentation equilibrium, was computed via SEDNTERP (22).

RESULTS

Comparison of FRET in Different Constructs. We prepared three YFP–myosin–CFP constructs that differed in the linker regions between the fluorescent protein and myosin (Figure 1). All of these constructs showed similar and substantial FRET between the YFP and CFP probes, as indicated by the sensitized YFP emission when excited at 436 nm (15). On the basis of the degree of CFP donor quenching (15), the FRET efficiency was estimated to be about 0.32 in the apo state at 1 M KCl and 0.58 at 40 mM KCl. This shift is due, at least in part, to the reduced YFP absorption at high chloride concentration. However, under both ionic conditions ATP addition caused little or no change in the observed emission spectra of all three constructs. Any change that was observed involved a small increase in YFP acceptor emission and decrease in CFP donor emission ($\leq 5\%$). These small changes were confirmed by time-resolved measurements in a stopped-flow apparatus (Supporting Information, Figure S1). The latter technique provided a more reliable way to measure small changes in emission intensity because it avoided drift in the signal between additions of ligand (e.g., due to photobleaching) and dilution errors. These results with our YFP–myosin–CFP construct are very different to those published for the GFP–myosin–BFP construct where a 40% quench in acceptor emission on ATP addition was noted (6). Subsequently, we obtained the DNA construct for the GFP–myosin–BFP construct and confirmed that this preparation showed a marked difference in the apparent FRET signal when compared in the same apparatus (Figure 2). Initially, we thought that the constructs differed in their response to ATP because of orientation differences between the pairs of probes. However, while this may be an important and contributing factor, we also noted that, in the case of the GFP–myosin–BFP construct, the change in the GFP signal contained a large non-FRET component. This was revealed by a 23% enhancement in GFP fluorescence on ATP addition when the GFP was excited directly at 485 nm, rather than via the BFP donor (Figure 3a). Furthermore, there were marked changes in the absorption spectra of the GFP–myosin–BFP construct on ATP addition (Figure 3b). Suzuki et al. (6, 23) used sensitized GFP emission to calculate the degree of FRET whereas the BFP donor fluorescence showed

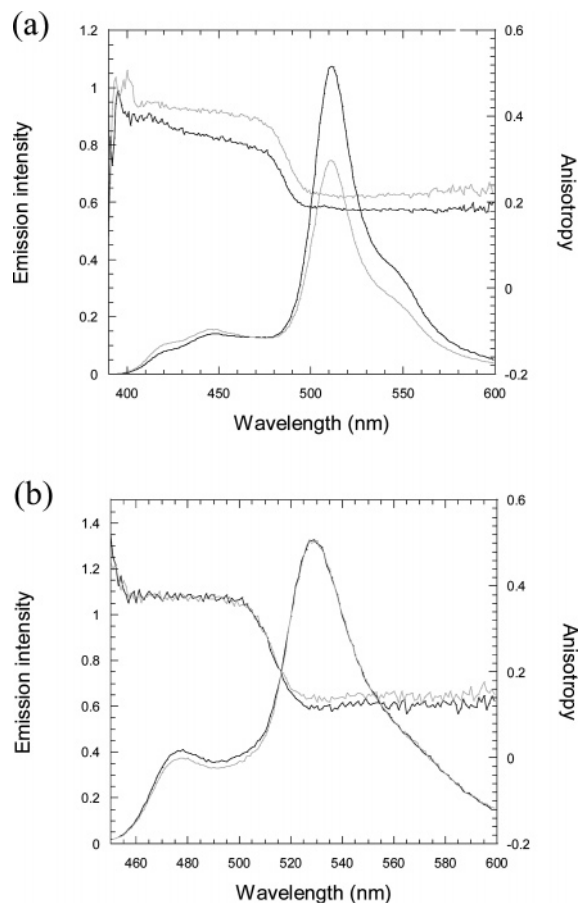


FIGURE 2: Steady-state FRET emission and anisotropy spectra in the absence (black line) and presence (gray line) of 1 mM ATP: (a) GFP–myosin–BFP on excitation at 380 nm; (b) YFP–myosin–CFP (0L) on excitation at 436 nm. Note the small and opposite effect of ATP on the donor intensity. The emission spectra were calculated from the total emission ($I_{||} + 2I_{\perp}$) and the anisotropy from $(I_{||} - I_{\perp})/(I_{||} + 2I_{\perp})$ after correction for the G -factor. Note that the anisotropy exceeds 0.4 at low wavelengths owing to a small contribution from light scattering. The anisotropy values are analyzed in Table 2.

much smaller changes in intensity, as we also observed (Figure 2). As discussed below, the latter provides a more robust measurement of FRET efficiency, while sensitized emission grossly overestimates the FRET change induced by ATP.

Determination of FRET Efficiency. Förster energy transfer can be quantified by two different approaches: (1) quenching of the donor fluorescence; (2) measurement of acceptor-sensitized emission (24). The former is a more direct method and requires measurement of the donor fluorescence emission intensity in the absence and presence of the acceptor. In the case of fluorescent protein FRET pairs, the acceptor can be effectively removed by selective proteolysis or denaturation of the intervening protein (i.e., myosin) or by photobleaching the acceptor. For the sensitized emission method, the acceptor signal intensity when excited via the donor is compared with direct excitation of the acceptor. This method requires knowledge of the relative absorption coefficients of the donor and acceptor, as well as the fluorometer spectral correction factors.

Donor quenching is usually assessed in microscope-based studies by photobleaching of the acceptor. When this was done with the GFP–myosin–BFP construct on a bulk scale

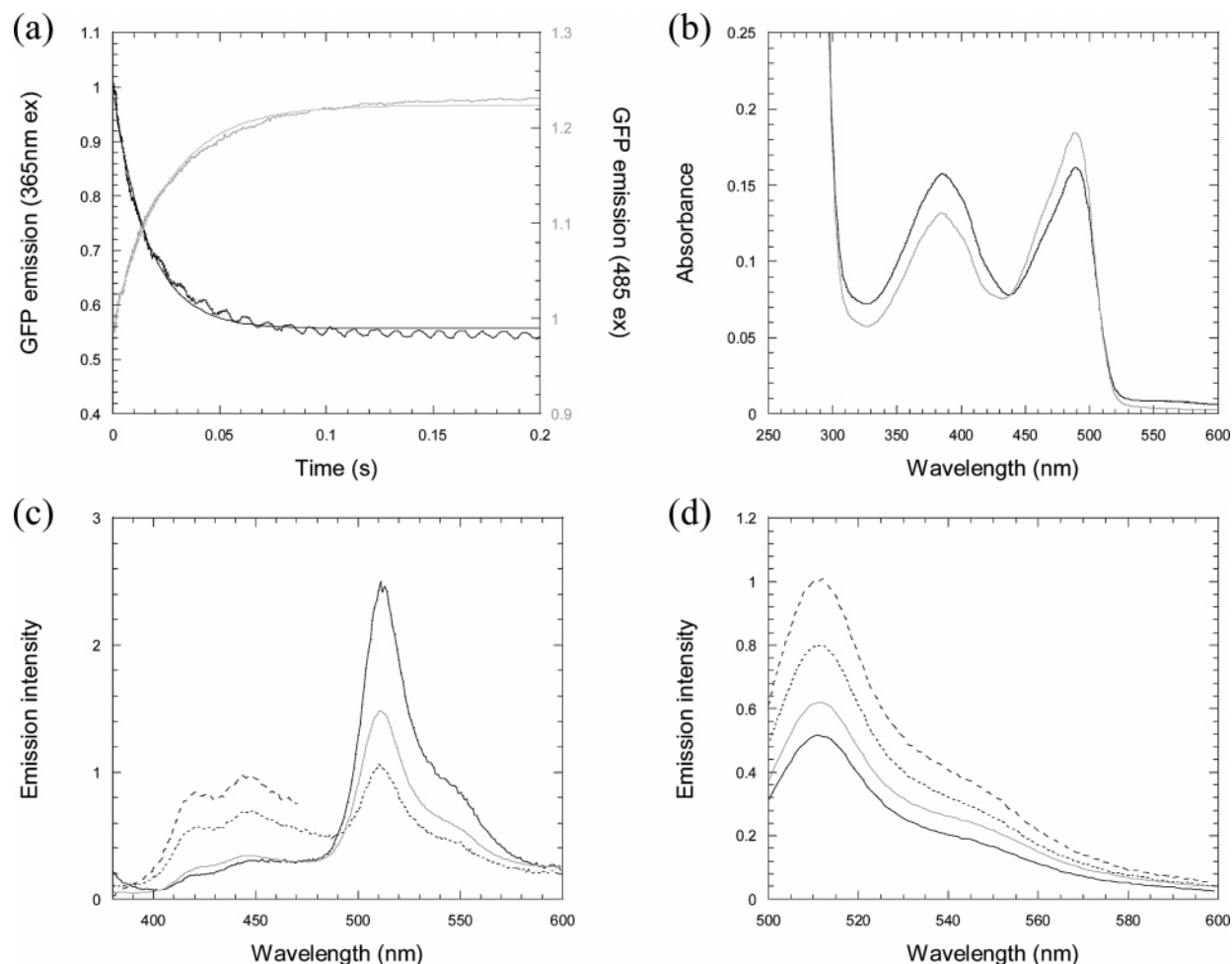


FIGURE 3: (a) Fluorescence stopped-flow records of 0.25 μM GFP-myosin-BFP on mixing with 500 μM ATP (reaction chamber concentrations). GFP emission was monitored at >515 nm with excitation at 365 nm (black line, apparent FRET from BFP) or directly at 485 nm (gray line). Fitted rate constants (single exponential) were 62 and 41 s^{-1} , respectively. The assays were carried out in 40 mM NaCl, 20 mM HEPES, and 2 mM MgCl_2 at pH 7.5 and 20 $^\circ\text{C}$. (b) Absorption spectra of 3.1 μM GFP-myosin-BFP in the absence (black line) and presence (gray line) of 280 μM ATP. The latter was recorded within 1 min of addition of the ATP. (c) Fluorescence emission spectrum of 1 μM GFP-myosin-BFP (excitation at 365 nm) before (black solid line) and after (dotted line) 2 h digestion with 0.1% (w/w) trypsin. Assuming that 100% digestion of the myosin and/or linker regions would reduce the GFP FRET emission peak at 510 nm to the baseline level, the reaction was 58% complete at 2 h. On 100% digestion, the BFP emission peak can be calculated (dashed line) for that in the absence of any quenching from FRET or intramolecular association with GFP. Also shown (gray line) is the spectrum of GFP-myosin-BFP in the presence of ATP from a separate experiment that was normalized to give a similar enhancement in BFP emission as seen in (a). (d) Same samples as in (c) but using direct excitation of the GFP at 480 nm. Again, the signal in the absence of any interaction (dashed line) is calculated assuming the spectrum at 2 h (dotted line) represents 58% completion.

using a 120 mW argon ion laser tuned to 488 nm, loss of the GFP fluorescence was accompanied by at most a 20% increase in BFP fluorescence (Supporting Information, Figure S2). However, acceptor photobleaching underestimates the degree of FRET in this case (2). When the GFP-myosin-BFP construct was treated with trypsin, there was a $>200\%$ rise in BFP fluorescence and fall in GFP acceptor fluorescence (Figure 3c), which allowed a better estimate of the FRET efficiency (Table 1). Unfortunately, proteolysis was accompanied by a rise in turbidity. For this reason, the limit of BFP emission at 100% proteolysis was calculated from the observed value at 58% proteolysis where the turbidity was less extensive by assuming the GFP-sensitized emission decreased to 0 at 100% proteolysis. On the basis of these data, the effect of ATP on the FRET efficiency of the GFP-myosin-BFP construct was rather small (0.70–0.66) compared to the values calculated by Suzuki et al. (6) of 0.439–0.082 [obtained from the sensitized emission procedure (23)]. We also obtained a larger ATP-induced change using this

method with our data (Table 1). What is the basis of this discrepancy? As noted above, we found there was a large ground-state perturbation of the GFP spectrum (and possibly the BFP spectrum) that we attribute to intramolecular association of the fluorescent proteins, and this complicates the analysis of the FRET efficiency.

Absorption and Fluorescence Changes Arising from Intramolecular Association. The absorption spectrum of the GFP-myosin-BFP construct revealed two peaks (380 and 488 nm) as expected (Figure 3b), but their absorbance values were approximately equal rather than the 1:2.8 ratio expected from the absorption coefficients of isolated BFP and GFP, respectively (10). On digestion of the myosin/linker region with trypsin, the 488 nm peak increased in intensity, while the 380 nm peak decreased. Unfortunately, the accompanying rise in turbidity prevented a quantitative analysis, but after an approximate baseline correction, the ratio of peak heights approached the expected 1:2.8 ratio. Digestion of GFP-myosin-BFP with trypsin was accompanied by a rise in GFP

Table 1: Estimation of FRET Efficiencies for the GFP–Myosin–BFP Construct^a

	donor quenching using method			sensitized emission using method		
	a	b	c	d	e	f
apo	0.57	0.70	0.18	0.25	0.438	0.349
+ATP	0.51	0.66	0.06	0.13	0.082	0.079

^a FRET efficiencies were calculated using several different methods. Methods a–c are based on donor quenching ($FRET = 1 - F_{DA}/F_D$, where F_{DA} and F_D = donor emission intensity in the presence and absence of an acceptor, respectively), and methods d–f are based on the sensitized emission intensity [$FRET = [(F_{FRET}/F_{dir}) - (\epsilon^{A_{365}}/\epsilon^{A_{488}})](\epsilon^{A_{488}}/\epsilon^{D_{365}})$, where F_{FRET}/F_{dir} = ratio of GFP emission intensity at 510 nm when excited via BFP at 365 nm to that excited directly at 488 nm (after correction for fluorometer excitation intensity at 365 and 488 nm), $\epsilon^{A_{365}}$ and $\epsilon^{A_{488}}$ = GFP molar absorption coefficients at 365 and 488 nm, respectively, and $\epsilon^{D_{365}}$ = BFP molar absorption coefficient at 365 nm]. Method a: observed FRET after limited proteolysis of the myosin/linker by trypsin. Method b: calculated FRET for 100% proteolysis. Method c: attempted GFP photolysis by 488 nm irradiation (see Supporting Information). Method d: apparent FRET calculated from sensitized emission. Method e: from Suzuki et al. (6). Method f: from Suzuki et al. (23). The most reliable estimate of the FRET efficiency is given by method b. The sensitized emission signal includes a contribution from non-FRET processes (see text). For the YFP–myosin–GFP constructs, the FRET efficiency for the apo state was estimated as 0.58 from donor quenching and selective denaturation of the myosin using 1 M GuHCl.

fluorescence when directly excited at 480 nm (Figure 3d). We propose that the absorbance of GFP at 488 nm in the intact construct is suppressed because of intramolecular association between the BFP and GFP moieties.

Early studies on wild-type GFP showed that self-association at high protein concentrations gave a spectral change (peak around 390 nm) similar to that produced by protonation (11). The phenomenon was confirmed and quantified in later studies to give a K_d for the dimer of 60 μ M (25). We observed the same effect of concentration with isolated eGFP (i.e., the mutant used in the GFP–myosin–BFP construct) but not isolated YFP 10C (Figure 4a,b). This was a surprising result given that both proteins are reported to dimerize with K_d values in the region of 100 μ M (10, 26). Furthermore, YFP has a higher pK than GFP and hence is more susceptible to protonation by external solvent (10). We therefore checked these preparations for dimerization using sedimentation equilibrium analysis and confirmed that both eGFP and YFP 10C dimerize with similar affinities (Figure 4c,d). Protonation of fluorescent proteins is a complex reaction and involves slow (millisecond to second time scale) isomerizations of the protein and/or chromophore (18). Association of these proteins at high concentrations presumably affects the conformation of the protein which, for GFP at least, affects the apparent pK of the chromophore. Note that even at eGFP concentrations $\gg K_d$, the anionic peak remains dominant, with a calculated A_{488}/A_{398} ratio of 1.5 for the dimer species (the ratio at low GFP concentrations was 7.5). This suggests that dimers of the type GFPH–GFP[−] are prevalent. A significant GFP protonated peak was observed even at pH 9.0 over the same concentration range as used in Figure 4a, suggesting that the ratio of protonated to anionic states reflects predominantly an internal proton rearrangement rather than a change in the external pK.

If the fluorescent proteins associate in the apo GFP–myosin–BFP construct, then the decrease in the 488 nm

absorbance could be due to the reduction in the GFP[−] anion while apparent increase in the BFP absorbance peak at 380 nm could arise from the protonated GFPH form, which absorbs in this region (395 nm). The BFP spectrum itself may also be perturbed on association with GFP (the turbidity change prevented accurate separation of the BFP and GFPH peaks). These ground-state perturbations have a strong influence on the apparent FRET signal. ATP addition is accompanied by significant absorption changes (15%) in the GFP–myosin–BFP construct (Figure 3b), in a direction that suggests there is less intramolecular probe association. These ground-state changes are accompanied by changes in fluorescence emission intensities that operate in conjunction with genuine FRET changes. We have not seen any ATP-induced changes in GFP fluorescence in single fusions to the myosin II motor domain (27), supporting the idea that intramolecular association is involved. We consider that the large ATP-induced enhancement in GFP fluorescence, observed when the GFP–myosin–BFP construct was excited directly at 488 nm, arises from a shift in the relative amounts of the GFPH and GFP[−] states toward the anionic state. In the apo state, the high apparent FRET efficiency calculated from the sensitized emission arises because GFPH is excited at similar wavelengths as for BFP, and this species emits at 510 nm owing to an efficient excited-state proton transfer process (see Discussion). We did not detect any absorption changes on addition of ATP to YFP–myosin–CFP constructs.

Evidence for an Equilibrium between States. We propose that when fluorescent proteins are in close proximity, there is a tendency for them to associate with each other. This is apparent in the GFP–myosin–BFP construct because of the shift in GFP protonation, but the process may go undetected in the case of the YFP–myosin–CFP constructs. If an equilibrium exists between the ionized and protonated GFP states, then this is potentially perturbable in relaxation experiments. Interestingly, in temperature-jump studies, a 3.6% decrease in the GFP emission signal was observed on excitation at 365 nm, when the temperature was rapidly increased from 15 to 25 °C. A much smaller change (−0.6%) was observed in the presence of ATP (Figure 5a). Given that a 10 °C temperature jump is likely to shift the equilibrium concentrations by only a small degree, signals of this magnitude indicate that the interconverting species have a large difference in their fluorescence emission intensity and both are present in significant amounts (i.e., the equilibrium is near unity).

If the fluorescent proteins associate with each other, they could lock the N- and C-terminal domains of myosin and possibly perturb the conformational changes associated with the myosin domain. Tryptophan fluorescence provides a sensitive means of monitoring the intrinsic conformational changes within myosin, particularly the signal from W501, which reports on a conformational transition coupled to the hydrolysis step (16, 19). Tryptophan emission was monitored free of any contribution from the probe fluorescence by using a WG320/UG11 filter combination. All constructs showed a tryptophan enhancement and yielded a rate constant of 30–40 s^{−1} at saturating ATP, close to the values of the wild-type and W501+ *Dd* motor domains (16, 28). The apparent FRET signal from the GFP–myosin–BFP construct also showed a phase with essentially the same rate constant at saturating ATP, as was previously reported by Suzuki et al.

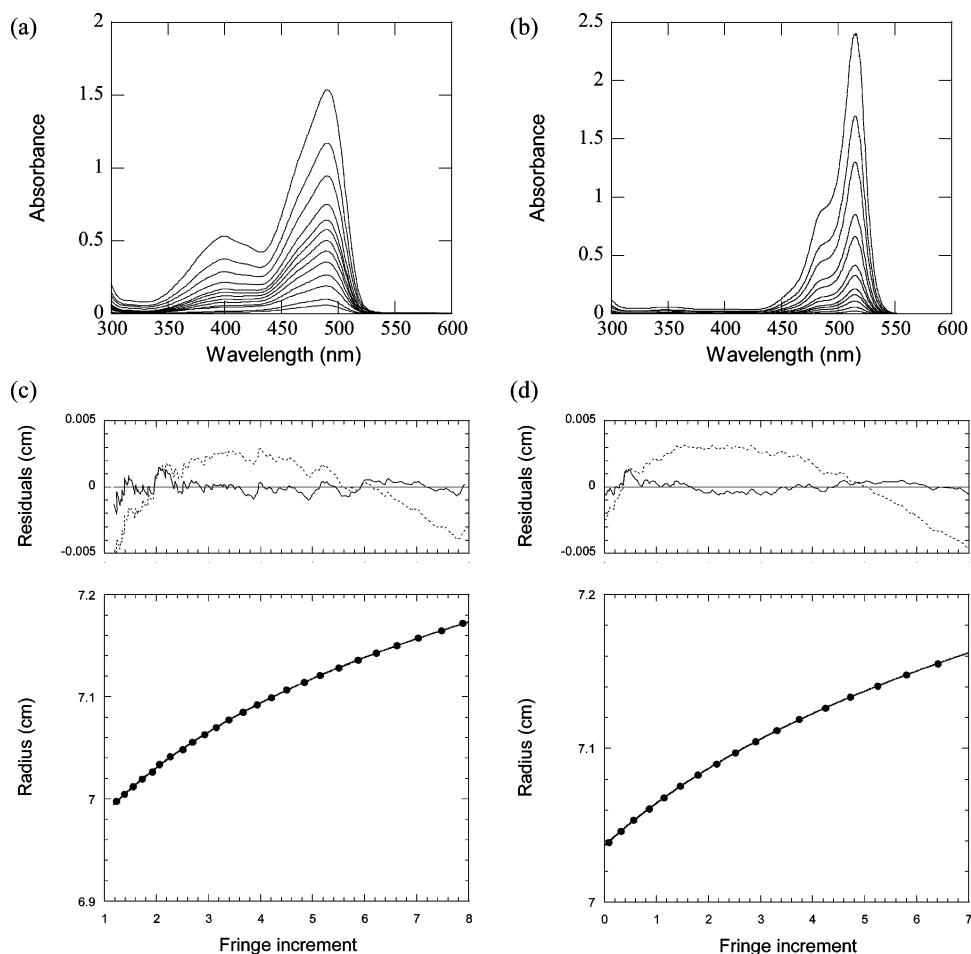


FIGURE 4: (a) Absorption spectra of isolated eGFP over a concentration range of 7–293 μM measured in a 1 mm path length cell. Fitting the A_{488} and A_{395} values as a function of concentration yielded a K_d value of 335 μM for dimerization (Supporting Information, Figure S3), but the value was ill-defined as it co-varied with the absorption coefficients assigned to the dimer species. Force fitting the absorption data with a $K_d = 237 \mu\text{M}$ [see (c) below] gave a rise of only 3% increase in the variance of the fit and yielded absorption coefficients of the dimer of 47 and 27 $\text{mM}^{-1} \text{cm}^{-1}$ at 488 and 395 nm, respectively. (b) Similar measurement for isolated YFP 10C (2.6–287 μM). (c) Sedimentation equilibrium profile for eGFP yielding a K_d of $237 \pm 36 \mu\text{M}$ and a second virial coefficient $2\text{BM} = 40.9 \text{ mL g}^{-1}$. Only one-tenth of the data points are plotted so that the fitted line is visible. The residual plot shows the deviation for the best fit (solid line) and a model in which no association occurs (dotted line). (d) Sedimentation equilibrium profile for YFP yielding a K_d of $101 \pm 19 \mu\text{M}$ and $2\text{BM} = 18.6 \text{ mL g}^{-1}$. Residual plot as in (c).

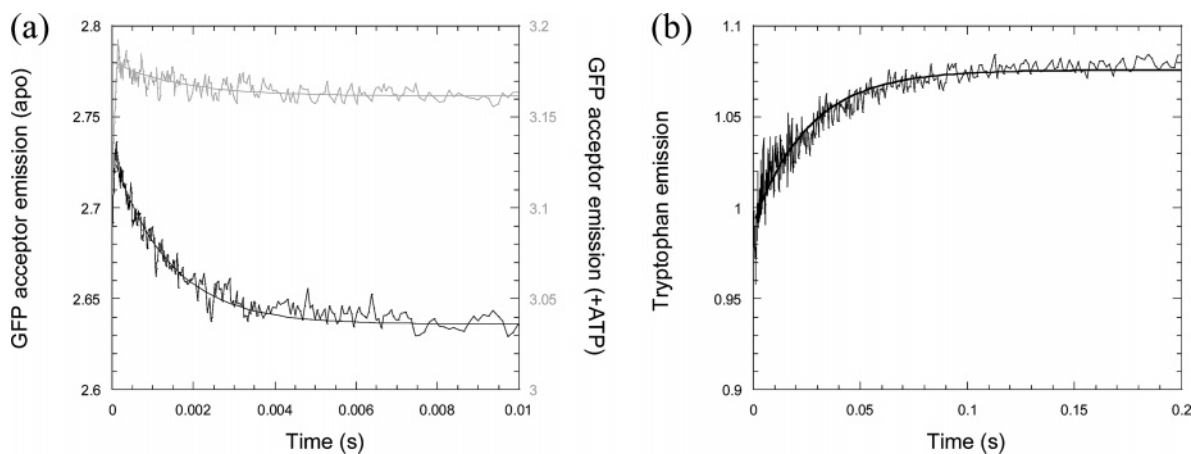


FIGURE 5: (a) Temperature-jump fluorescence records for 1 μM GFP–myosin–BFP in 100 mM NaCl (additional salt needed for efficient Joule heating), 20 mM HEPES, and 2 mM MgCl_2 at pH 7.5 and 15 $^\circ\text{C}$ start temperature (final temperature $\approx 25 \text{ }^\circ\text{C}$). The black trace is the apo state ($k_{\text{obs}} = 725 \text{ s}^{-1}$, amplitude = -3.6%), and gray trace is in the presence of 1 mM ATP ($k_{\text{obs}} = 585 \text{ s}^{-1}$, amplitude = -0.6%). The sample was excited at 365 nm and emission at $>515 \text{ nm}$ was captured and thus represents the apparent FRET signal between BFP and GFP. (b) Fluorescence stopped-flow record of 0.25 μM GFP–myosin–BFP on mixing with 500 μM ATP. Tryptophan fluorescence was monitored by excitation at 297 nm and emission monitored between 320 and 380 nm. Fitted rate constant = 38 s^{-1} .

(6). These results do not rule out an association between the probes but show that any such association does not have a

significant effect on conformational changes within the motor domain. The change in the apparent BFP–GFP FRET signal

Table 2: Analysis of Fluorescence Anisotropy Data^a

construct	anisotropy			polarization factors				dipole angle	orientation factor		critical Förster distance	
	r_D	r_T	r_A	$\langle d^2_D \rangle$	$\langle d^2_T \rangle$	$\langle d^2_A \rangle$	d^2_T	θ_T	$\kappa^2(\text{low})$	$\kappa^2(\text{high})$	$R_0(\text{low})$ (nm)	$R_0(\text{high})$ (nm)
GFP–myosin–BFP	0.36	<i>0.18</i>	0.37	0.90	<i>0.45</i>	0.93	<i>0.54</i>	33.6	<i>0.1</i>	3.2	3.0	5.3
+ATP	0.39	<i>0.22</i>	0.37	0.97	<i>0.55</i>	0.93	<i>0.61</i>	30.7	<i>0.05</i>	3.4	2.6	5.3
YFP–myosin–CFP (0L)	0.38	0.12	0.32	0.95	0.30	0.8	0.39	39.4	0.1	3.0	3.3	5.9
+ATP	0.38	0.14	0.32	0.95	0.35	0.8	0.46	36.8	0.1	3.1	3.3	5.9
YFP–myosin–CFP (2L)	0.37	0.10	0.27	0.92	0.26	0.68	0.41	38.7	0.2	2.6	3.7	5.7
+ATP	0.37	0.11	0.27	0.92	0.27	0.68	0.43	38.1	0.2	2.6	3.7	5.7

^a The anisotropy of the BFP/CFP donor (r_D) and GFP/YFP acceptor (r_A) and the FRET emission (r_T) were measured as described in Figure 2. The corresponding polarization factors were calculated by dividing by 0.4, and the axial transfer depolarization factor was calculated with d^2_T from the relationship $\langle d^2_T \rangle = \langle d^2_D \rangle d^2_T \langle d^2_A \rangle$ (30). The angle between the donor emission dipole and the acceptor absorption dipole, θ_T , is given by $d^2_T = (3 \cos^2 \theta_T - 1)/2$. The lower and upper limits of κ^2 were read off from the contour plots of Dale et al. (30) for the appropriate d^2_T value. The upper and lower limits for the critical Förster distance, R_0 , were calculated using the parameters of Hink et al. (14) in combination with the κ^2 limits. In the case of transfer polarization with the GFP–myosin–BFP complex, the values (in italics) are dominated by ESPT and lead to further uncertainties in R_0 (see text).

arising from protein association and protonation reactions (Figure 5a) is faster than the apparent ATP hydrolysis step (Figure 5b), so that the former remains a suitable empirical probe of the latter.

Fluorescence Anisotropy Measurements. The steady-state fluorescence emission anisotropy of isolated GFP and its variants is close to 0.3 (27, 29) and is in line with the value predicted from the rotational correlation time of a cylindrical protein with 2.4 nm diameter and 4.2 nm length. Fusing GFP to another protein will only serve to restrict this motion further, leading to potentially higher anisotropy values. Steady-state anisotropies of ≥ 0.3 for the donor and acceptor fluorophores will give rise to a large uncertainty in the κ^2 value (30). Limits can be placed on the κ^2 value, particularly if the depolarization of the FRET signal is determined. However, as the anisotropies of the donor and acceptor approach 0.4, the value for the FRET depolarization value has a rather limited effect on reducing the uncertainty in κ^2 . We determined the anisotropy spectra for the myosin constructs, at the same time as calculating the polarization-corrected emission spectra shown in Figure 2.

The anisotropy of the donor (BFP or CFP) emission was high (≥ 0.36) whereas that of the apparent FRET-induced acceptor emission anisotropy was much lower (0.10–0.22). When the GFP or YFP acceptor was excited directly, the anisotropies were 0.37 and 0.32, respectively. The depolarization of FRET-based fluorescence is a commonly observed property and is a result of the finite angle (θ_T) between the mean donor emission and acceptor absorption dipoles (30). Using the values for the donor, acceptor, and FRET anisotropies and the calibration curves of Dale et al. (30), the range of potential κ^2 values lies between about 0.1 and 3 in both the GFP–myosin–BFP and YFP–myosin–CFP (2L) complexes (Table 2). The effect of these κ^2 values on the critical Förster distance, R_0 , is also given in Table 2. It is evident that the uncertainty in R_0 is > 2 nm for all constructs, whereas the calculated distance change (naively assuming no change in κ^2) on adding ATP to the constructs is < 0.2 nm based on the change in donor quenching. It is evident that the lever arm swing cannot be quantified in the manner employed by Suzuki et al. (6).

In the case of the GFP–myosin–BFP construct, the observed emission has a dominant contribution from the GFPH state. Independent experiments on the anisotropy of isolated eGFP at 510 nm and high protein concentration (1

mM) gave values of 0.12 and 0.33 when excited at 390 and 488 nm, respectively. The lower value for the anisotropy for the GFPH state relative to the GFP[−] anion could arise from a difference in the angle of their absorption dipoles (estimated to be about 13° in ref 31) relative to the GFP[−] emission. However, contributions from homo-FRET and absorption and re-emission complicate this analysis. The true value of d^2_T for the FRET-based component in the GFP–myosin–BFP construct is therefore undetermined and could be higher than that given, but this only marginally increases the large uncertainty in κ^2 reported in Table 2.

In an attempt to explore the dipole orientation problem further, myofibrils were decorated with the fusion proteins so as to orient the probe molecules with respect to the actin filaments (32). Under a fluorescence microscope equipped with polarization optics in the excitation channel, only a small difference was seen in the dichroism ratio between myofibrils aligned with or 90° to the plane of polarization (see Supporting Information, Figure S4). Either the probes lie within a few degrees of the magic angle or, more likely, they are somewhat statically disordered over a range close to the magic angle. Thus no decisive information could be gleaned from this approach.

DISCUSSION

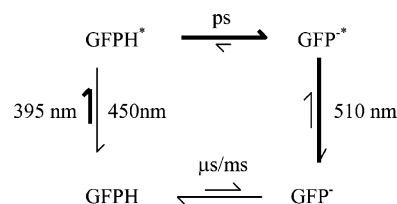
We have compared the apparent ATP-induced changes in FRET between GFP-type probes attached to the N- and C-termini of the *Dd* myosin motor domain II in constructs that differ in three fundamental ways: (1) the nature of the motor domain, (2) the nature of the linkers, (3) the color variants of the FRET pairs. The first difference is unlikely to be a major factor. The GFP–myosin–BFP clone is based on the wild-type *Dd* motor domain whereas the YFP–myosin–CFP constructs are based on a single tryptophan mutant W501+ that has three W to F substitutions. Previous studies have shown the kinetic mechanism of the ATPase of these constructs to be very similar (16, 28). Most importantly, all these constructs show a characteristic ATP-induced signal change with a rate constant of 30–40 s^{−1} at 20 °C at near saturating [ATP]. This transition appears to be characteristic of the conformational change that is coupled to the hydrolysis reaction and is believed to control the swing of the C-terminal domain and lever arm, when present (33). The relative movements of the myosin N- and C-termini are therefore likely to be the same in all constructs,

although the response of the attached probes is clearly different.

The linker regions differ significantly and could contribute to the different flexibility and orientation of the probes. This could affect the value of κ^2 and the ability of the probes to undergo intramolecular association. The first construct we made contained GGG linkers between both YFP and CFP and the myosin motor domain (Figure 1), in an attempt to duplicate the original GFP–myosin–BFP construct of Suzuki et al. (6). However, our constructs contain an additional methionine in the C-terminal linker and a methionine–lysine substitution in the N-terminal linker owing to the different cloning strategy used. Subsequently, Sasaki et al. (17) reported that the N-terminal linker in their construct was actually GPG, and we confirmed this sequence for the GFP–myosin–BFP construct that was supplied to us by the Sutoh laboratory. In the case of the YFP–myosin–CFP constructs, removing the GGG linkers had little effect on the degree of FRET and its sensitivity to ATP. However, the C-terminus of GFP contains eight residues that are not resolved in crystal structures and therefore could contribute to the flexibility of the myosin N-terminal linker in the absence of a GGG sequence. The residues in the C-terminal linker are compatible with helix formation, and therefore this link could allow the BFP or CFP to form an artificial lever arm (cf. ref 34), particularly in the absence of the GGG residues. Miyawaki and Tsien (2) comment on the observation that markedly different FRET efficiencies are seen in chimera constructs designed as Ca^{2+} sensors, where the linker region differs by the addition of a single amino acid. They conclude that a change in orientation rather than change in distance of separation of the probes is the dominant factor. This could account for the different direction of the FRET change on ATP addition for the GFP–myosin–BFP and YFP–myosin–CFP constructs studied here. It is evident that the distance change calculated from the small change in donor quenching (<5%) corresponds to <0.2 nm movement if κ^2 were constant (an unlikely scenario), which is much smaller than the >2 nm uncertainty in R_0 (and hence r) if κ^2 changed. Attempts to define a more restricted range of possible orientations by immobilizing the whole chimera on oriented actin filaments within myofibrils revealed a small deviation from isotropic behavior, but the conclusion remains ambiguous (see Supporting Information). This contrasts with the studies of Yan and Marriott (32), where covalently attached rhodamine and fluorescein tags on actin showed substantial alignment with the actin filament axis and allowed more rigorous limits to be applied to the κ^2 value.

The final factor to consider is the different GFP variants used. At first sight, these proteins might be expected to behave similarly because they are based on a conserved and stable β -barrel structure. Most mutations to generate the color variants are internal and close to or within the *p*-hydroxybenzylideneimidazolidinone fluorophore (10). However, we show here that although YFP 10C and eGFP have a similar tendency to dimerize, in line with previous studies (26), only with eGFP does this reaction have a significant effect on the proportion of the protonated state. The perturbed absorption spectrum of the GFP–myosin–BFP construct is consistent with the formation of a significant concentration of GFPH in the apo state. If it is assumed that the true FRET change on ATP addition is revealed in the dequenching of

Scheme 1



BFP fluorescence, then the observed >30% change in the apparent sensitized GFP emission comprises a dominant contribution of >25% from non-FRET origins. Therefore, we consider that the majority (>80%) of the 510 nm emission observed when apo GFP–myosin–BFP is excited at 380 nm arises from GFPH emission rather than FRET from BFP.

The proposal that intramolecular association of the GFP with BFP in the GFP–myosin–BFP construct leads to a paradoxical situation that as the probes become close enough to associate with each other (chromophore separation about 3.6 nm), the degree of genuine FRET will fall because GFPH is a poor acceptor for the BFP excited-state energy (the overlap integral is about $1/5$ that of the GFP^- anion). However, GFPH predominantly emits at 510 nm when excited at wavelengths below 400 nm owing to a very efficient excited-state proton transfer reaction (29), as shown in Scheme 1.

This signal would complement the genuine BFP to GFPH FRET signal to give the appearance of a very efficient FRET process. YFPH also undergoes an excited-state proton transfer reaction, but the process is much less efficient than for GFPH because the dominant route for decay of the YFPH* excited state is back to YFPH via a nonradiative pathway (18). Furthermore, on dimerization of isolated YFP, there is little indication of the formation of YFPH. It is therefore possible that YFP and CFP associate in the YFP–myosin–CFP constructs but the process is optically silent.

The dimerization of GFP is a well-known phenomenon, and the consequential shift toward the protonated state was noted for wild-type GFP many years ago (11). Dimerization of YFP was inferred from the fall in anisotropy of concentrated YFP from 0.4 to 0.28 on the picosecond time scale owing to homo-FRET (35). These studies concluded that the chromophores were within favorably oriented for FRET ($\kappa^2 = 3.8$) and the proteins were in contact near the equators of their β -barrels. It is likely, though not proven, that the protein pairs lie in an antiparallel manner, as observed in the crystal structures. However, in the FRET constructs tethering of the N- and C-termini would favor parallel stacking. This difference would contribute to the (generally unknown) entropic factors relating inter- and intramolecular interactions (36). Surface mutations which reduce intermolecular association (26) will therefore not necessarily overcome the problems of intramolecular association.

It is possible that the myosin fusion constructs have a higher tendency to dimerize intermolecularly through the probe molecules (i.e., the probes form a dimer of dimers) than isolated GFP or YFP. We have found that the YFP–myosin–CFP construct at submicromolar concentrations is more effective at bundling actin than the myosin construct alone.

The temperature-jump studies with GFP–myosin–BFP (Figure 5a) show a large signal change in the apo state

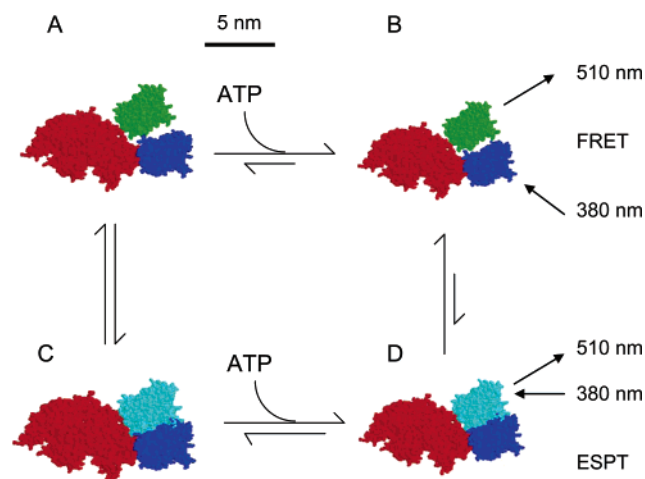


FIGURE 6: Schematic diagram to show the influence of probe association on GFP–myosin–BFP conformation. FRET measurements have been used in an attempt to quantify the lever arm movement induced by ATP (reaction A to B) (6). Aside from the undetermined influence of orientation on the FRET efficiency, the data of Figure 3b indicate that the ground-state properties of GFP (green) and possibly BFP (blue) are perturbed, as could arise by probe association (states C and D). The association between GFP and BFP induces the protonated state, GFPH (cyan), particularly in the apo state (C). On excitation at 380 nm, GFPH emits at 510 nm following rapid excited-state proton transfer (ESPT), giving the appearance of FRET. Molecular shapes for the myosin motor domain (red) and GFP/BFP are based on crystal structures 2MYS (41) and 1EMB (42), respectively.

indicating that the equilibrium constant is poised close to unity. While this result could represent two states of the lever arm in the apo state, we consider that the signal primarily reflects a change in intramolecular association of the GFP and BFP (and hence a change in the proportion of GFPH). The lever arm itself is probably not in dynamic equilibrium in the apo state because no perturbation of the tryptophan fluorescence response of the W501+ construct was observed by temperature or pressure jump, but changes were observed in the presence of ATP corresponding to a lever arm movement (19). These considerations give rise to the model shown in Figure 6 whereby the observed optical changes with GFP–myosin–BFP changes reflect both FRET and ESPT, with ATP reducing the tendency for intramolecular association. The actual change in separation of the probe chromophores in response to ATP is difficult to calculate owing to the wide range of potential κ^2 values and could range from 0 to more than 2 nm. Although the GFP–BFP FRET pair is no longer favored because of the poor photostability of BFP, this pair was used recently to characterize subdomain interactions in dynein (37). It is noteworthy that in these experiments the GFP emission showed a much larger response to ATP addition than the BFP emission, again suggesting that a large non-FRET component is present.

Absorption spectra of the currently favored FRET pair of CyPET–YPet were not published, so it is difficult to assess if non-FRET processes play a significant part in the large observed fluorescence change on separation of the probes by trypsin cleavage (4). The new generation of red fluorescent proteins (38) has not been used extensively for FRET measurements due their wide absorption bands. Some of these proteins are reported to remain monomeric at high concentration and have a low pK , but neither factor is

guaranteed to rule out formation of the protonated state by internal proton movement on intramolecular association. Each FRET pair should be tested on a case-by-case basis. The majority of FRET studies using fluorescent protein pairs have been carried out only at a cellular level by microscopy rather than by *in vitro* spectroscopic measurements with expressed proteins, so that these potential problems could have gone undetected. An appropriate control for the behavior of the donor or acceptor in the absence of FRET from the partner probe would use constructs in which the partner is rendered colorless by mutation (39). In this case, perturbations arising from intramolecular association should still be evident. Although the spectra of the YFP–myosin–CFP constructs do not appear to be perturbed by intramolecular association, previous studies have shown that photobleaching of YFP under the microscope can, in itself, lead to anomalous FRET results (2, 18, 40).

ACKNOWLEDGMENT

We thank Dr. Bob Dale for discussions regarding anisotropy.

SUPPORTING INFORMATION AVAILABLE

Figure S1, stopped-flow fluorescence records of YFP–myosin–CFP and GFP–myosin–BFP on mixing with ATP; Figure S2, acceptor photobleaching of GFP–myosin–BFP; Figure S3, analysis of the GFP dimerization constant from absorption data; and Figure S4, dichroism of myofibrils labeled with GFP–myosin–BFP. This material is available free of charge via the Internet at <http://pubs.acs.org>.

REFERENCES

- Periasamy, A., and Day, R. N. (1999) Visualizing protein interactions in living cells using digitized GFP imaging and FRET microscopy, *Methods Cell Biol.* 58, 293–314.
- Miyawaki, A., and Tsien, R. Y. (2000) Monitoring protein conformations and interactions by fluorescence resonance energy transfer between mutants of green fluorescent protein, *Methods Enzymol.* 327, 472–500.
- Raicu, V., Jansma, D. B., Miller, R. J., and Friesen, J. D. (2005) Protein interaction quantified *in vivo* by spectrally resolved fluorescence resonance energy transfer, *Biochem. J.* 385, 265–277.
- Nguyen, A. W., and Daugherty, P. S. (2005) Evolutionary optimization of fluorescent proteins for intracellular FRET, *Nat. Biotechnol.* 23, 355–360.
- Periasamy, A., and Day, R. N. (2005) in *Methods in Physiology Series*, p 312, Oxford University Press, Oxford.
- Suzuki, Y., Yasunaga, T., Ohkura, R., Wakabayashi, T., and Sutoh, K. (1998) Swing of the lever arm of a myosin motor at the isomerization and phosphate-release steps, *Nature* 396, 380–383.
- Riven, I., Kalmanzon, E., Segev, L., and Reuveny, E. (2003) Conformational rearrangements associated with the gating of the G protein-coupled potassium channel revealed by FRET microscopy, *Neuron* 38, 225–235.
- Schaufele, F., Wang, X., Liu, X., and Day, R. N. (2003) Conformation of CCAAT/enhancer-binding protein alpha dimers varies with intranuclear location in living cells, *J. Biol. Chem.* 278, 10578–10587.
- Kerschensteiner, D., Soto, F., and Stocker, M. (2005) Fluorescence measurements reveal stoichiometry of K^+ channels formed by modulatory and delayed rectifier alpha-subunits, *Proc. Natl. Acad. Sci. U.S.A.* 102, 6160–6165.
- Tsien, R. Y. (1998) The green fluorescent protein, *Annu. Rev. Biochem.* 67, 509–544.
- Ward, W. W., Prentice, H. J., Roth, A. F., Cody, C. W., and Reeves, S. C. (1982) Spectral perturbations of the *Aequorea* green-fluorescent protein, *Photochem. Photobiol.* 35, 803–808.

12. Wachter, R. M., and Remington, S. J. (1999) Sensitivity of the yellow variant of green fluorescent protein to halides and nitrate, *Curr. Biol.* 9, R628–R629.
13. Patterson, G. H., Piston, D. W., and Barisas, B. G. (2000) Forster distances between green fluorescent protein pairs, *Anal. Biochem.* 284, 438–440.
14. Hink, M. A., Visser, N. V., Borst, J. W., van Hoek, A., and Visser, A. J. W. G. (2003) Practical use of corrected fluorescence excitation and emission spectra of fluorescent proteins in Forster resonance energy transfer (FRET) studies, *J. Fluoresc.* 13, 185–188.
15. Zeng, W., Conibear, P. B., Dickens, J. L., Cowie, R. A., Wakelin, S., Malnasi-Csizmadia, A., and Bagshaw, C. R. (2004) Dynamics of actomyosin interactions in relation to the cross-bridge cycle, *Philos. Trans. R. Soc. London, Ser. B: Biol. Sci.* 359, 1843–55.
16. Malnasi-Csizmadia, A., Woolley, R. J., and Bagshaw, C. R. (2000) Resolution of conformational states of *Dictyostelium* myosin II motor domain using tryptophan (W501) mutants: Implications for the open-closed transition identified by crystallography, *Biochemistry* 39, 16135–16146.
17. Sasaki, N., Ohkura, R., and Sutoh, K. (2003) *Dictyostelium* myosin II mutations that uncouple the converter swing and ATP hydrolysis cycle, *Biochemistry* 42, 90–95.
18. McAnaney, T. B., Zeng, W., Doe, C. F., Bhanji, N., Wakelin, S., Pearson, D. S., Abbyad, P., Shi, X., Boxer, S. G., and Bagshaw, C. R. (2005) Protonation, photobleaching, and photoactivation of yellow fluorescent protein (YFP 10C): a unifying mechanism, *Biochemistry* 44, 5510–5524.
19. Malnasi-Csizmadia, A., Pearson, D. S., Kovacs, M., Woolley, R. J., Geeves, M. A., and Bagshaw, C. R. (2001) Kinetic resolution of a conformational transition and the ATP hydrolysis step using relaxation methods with a *Dictyostelium* myosin II mutant containing a single tryptophan residue, *Biochemistry* 40, 12727–12737.
20. Luo, R., Mann, B., Lewis, W. S., Rowe, A., Heath, R., Stewart, M. L., Hamburger, A. E., Sivakolundu, S., Lacy, E. R., Bjorkman, P. J., Tuomanen, E., and Kriwacki, R. W. (2005) Solution structure of choline binding protein A, the major adhesin of *Streptococcus pneumoniae*, *EMBO J.* 24, 34–43.
21. Rowe, A. J. (2005) in *Analytical Ultracentrifugation: Techniques and Methods* (Scott, D. J., Harding, S. E., and Rowe, A. J., Eds.) RSC Publishing, Cambridge.
22. Laue, T. M., Shah, B. D., Ridgeway, T. M., and Pelletier, S. L. (1992) in *Analytical Ultracentrifugation in Biochemistry and Polymer Science* (Harding, S. E., Rowe, A. J., and Horton, J. C., Eds.) RSC Publishing, Cambridge.
23. Suzuki, Y. (2000) Detection of the swings of the lever arm of a myosin motor by fluorescence resonance energy transfer of green and blue fluorescent proteins, *Methods* 22, 355–363.
24. Clegg, R. M. (1992) Fluorescence resonance energy transfer and nucleic acids, *Methods Enzymol.* 211, 353–388.
25. Wiehler, J., Jung, G., Seebacher, C., Zumbusch, Z., and Steipe, B. (2003) Mutagenic stabilization of the photocycle intermediate of green fluorescent protein (GFP), *ChemBioChem* 4, 1164–1171.
26. Zacharias, D. A., Violin, J. D., Newton, A. C., and Tsien, R. Y. (2002) Partitioning of lipid-modified monomeric GFPs into membrane microdomains of live cells, *Science* 296, 913–916.
27. Wakelin, S., Conibear, P. B., Woolley, R. J., Floyd, D. N., Bagshaw, C. R., Kovacs, M., and Malnasi-Csizmadia, A. (2002) Engineering *Dictyostelium discoideum* myosin II for the introduction of site-specific fluorescence probes, *J. Muscle Res. Cell Motil.* 23, 673–683.
28. Kuhlman, P. A., and Bagshaw, C. R. (1998) ATPase kinetics of the *Dictyostelium discoideum* myosin II motor domain, *J. Muscle Res. Cell Motil.* 19, 491–504.
29. Chatteraj, M., King, B. A., Bublitz, G. U., and Boxer, S. G. (1996) Ultra-fast excited state dynamics in green fluorescent protein: multiple states and proton transfer, *Proc. Natl. Acad. Sci. U.S.A.* 93, 8362–8367.
30. Dale, R. E., Eisinger, J., and Blumberg, W. E. (1979) The orientational freedom of molecular probes. The orientation factor in intramolecular energy transfer, *Biophys. J.* 26, 161–193.
31. Rosell, F. I., and Boxer, S. G. (2003) Polarized absorption spectra of green fluorescent protein single crystals: transition dipole moment directions, *Biochemistry* 42, 177–183.
32. Yan, Y., and Marriott, G. (2003) Fluorescence resonance energy transfer imaging microscopy and fluorescence polarization imaging microscopy, *Methods Enzymol.* 360, 561–580.
33. Malnasi-Csizmadia, A., Dickens, J. L., Zeng, W., and Bagshaw, C. R. (2005) Switch movements and the myosin crossbridge stroke, *J. Muscle Res. Cell Motil.* 26, 31–37.
34. Tsiavalariis, G., Fujita-Becker, S., and Manstein, D. J. (2004) Molecular engineering of a backwards-moving myosin motor, *Nature* 427, 558–561.
35. Jung, G., Ma, Y. Z., Prall, B. S., and Fleming, G. R. (2005) Ultrafast fluorescence depolarisation in the yellow fluorescent protein due to its dimerisation, *ChemPhysChem* 6, 1628–1632.
36. Jencks, W. P. (1981) On the attribution and additivity of binding energies, *Proc. Natl. Acad. Sci. U.S.A.* 78, 4046–4050.
37. Kon, T., Mogami, T., Ohkura, R., Nishiura, M., and Sutoh, K. (2005) ATP hydrolysis cycle-dependent tail motions in cytoplasmic dynein, *Nat. Struct. Mol. Biol.* 12, 513–519.
38. Shaner, N. C., Campbell, R. E., Steinbach, P. A., Giepmans, B. N., Palmer, A. E., and Tsien, R. Y. (2004) Improved monomeric red, orange and yellow fluorescent proteins derived from *Discosoma* sp. red fluorescent protein, *Nat. Biotechnol.* 22, 1567–1572.
39. Calleja, V., Ameer-Beg, S. M., Vojnovic, B., Woscholski, R., Downward, J., and Larijani, B. (2003) Monitoring conformational changes of proteins in cells by fluorescence lifetime imaging microscopy, *Biochem. J.* 372, 33–40.
40. Valentin, G., Verheggen, C., Piolot, T., Neel, H., Coppey-Moisan, M., and Bertrand, E. (2005) Photoconversion of YFP into a CFP-like species during acceptor photobleaching FRET experiments, *Nat. Methods* 2, 801–801.
41. Rayment, I., Rypniewski, W. R., Schmidt-Base, K., Smith, R., Tomchick, D. R., Benning, M. M., Winkelmann, D. A., Wesenberg, G., and Holden, H. M. (1993) Three-dimensional structure of myosin subfragment-1: a molecular motor, *Science* 261, 50–58.
42. Brejc, K., Sixma, T. K., Kitts, P. A., Kain, S. R., Tsien, R. Y., Ormo, M., and Remington, S. J. (1997) Structural basis for dual excitation and photoisomerization of the *Aequorea victoria* green fluorescent protein, *Proc. Natl. Acad. Sci. U.S.A.* 94, 2306–2311.

BI060943U